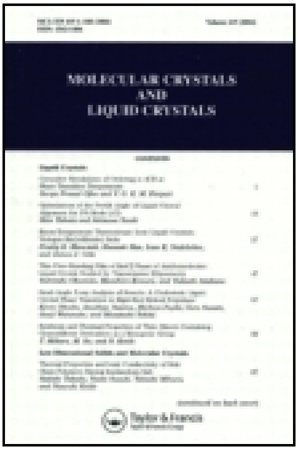

Molecular Crystals and Liquid Crystals
Publication details, including instructions for authors and subscription information:
http://www.tandfonline.com/loi/gmcl20

Diffraction From the Two Stable States in a Nematic Liquid Crystal cell containing a mono-grating with homeotropic director alignment

E. G. Edwards [a], C. V. Brown [a], E. E. Kriezis [a], S. J. Elston [a], S. C. Kitson [b] & C. J. P. Newton [b]

[a] Department of Engineering Science, University of Oxford, Oxford, United Kingdom

[b] HP Labs, Stoke Gifford, Bristol, United Kingdom

Version of record first published: 18 Oct 2010

Mol. Cryst. Liq. Cryst., Vol. 410, pp. 401/[929]–408/[936], 2004

ISSN: 1542-1406 print/1563-5287 online
DOI: 10.1080/15421400490433352

DIFFRACTION FROM THE TWO STABLE STATES IN A NEMATIC LIQUID CRYSTAL CELL CONTAINING A MONO-GRATING WITH HOMEOTROPIC DIRECTOR ALIGNMENT

E. G. Edwards, C. V. Brown, E. E. Kriezis and S. J. Elston
University of Oxford, Department of Engineering Science, Parks Road, Oxford, OX1 3JP, United Kingdom

S. C. Kitson and C. J. P. Newton
HP Labs, Filton Road, Stoke Gifford, Bristol, BS34 8QZ, United Kingdom

In this work we use the Q-tensor order parameter to express the elastic free energy of a nematic liquid crystal. This correctly preserves the $+n/-n$ symmetry and thus allows the modelling of defects. Using this, we calculate director profiles for cells containing surface relief gratings. Director profiles are presented which demonstrate that the cell supports two stable director configurations, in agreement with previous investigations [1–3]. The director profiles calculated are used in conjunction with Finite-Difference Time-Domain optical modelling to simulate the diffraction from the two stable states. The results of these simulations are then compared with experimental results for a cell fabricated with a relief grating on one internal surface. Diffraction strength is measured as a function of incident angle and as a function of incident polarisation.

Keywords: bistability; nematic liquid crystal; optical properties; Q-tensor

INTRODUCTION

Nematic liquid crystal cells containing surface relief gratings are of interest due to their capability of supporting more than one stable director

The authors would like to thank Dr L. A. Parry-Jones for useful discussions and the EPSRC and Hewlett-Packard for a CASE award for E. G. Edwards.

Address correspondence to E. G. Edwards, University of Oxford, Dept of Engineering Science, Parks Rd, Oxford, OX1 3JP, United Kingdom.

configuration. In this paper we investigate the geometry that supports zenithal bistability, which has been discussed in refs. [1–5]. This consists of a cell where one internal surface is flat and the other carries a monograting. The basic forms of the two stable states are shown in Figure 1. The flat surface and the grating are treated with an alignment layer, which gives homeotropic alignment. In this configuration the liquid crystal can lie either in a high tilt defect-free state or a low tilt defect-containing state. The precise structure of the director field will, of course, depend on the shape of the grating itself. In the first part of this paper we describe how the director profiles can be simulated.

In the second part of this paper we turn our attention to the optical properties of the states. We have already observed [6] that the diffraction strength from this type of cell is a useful measurable quantity. Here we investigate the diffraction strength as a function of incident angle and also as a function of incident polarisation. We are able to model the measurements by combining director profile simulations with Finite-Difference Time-Domain (FDTD) optical modelling software [7].

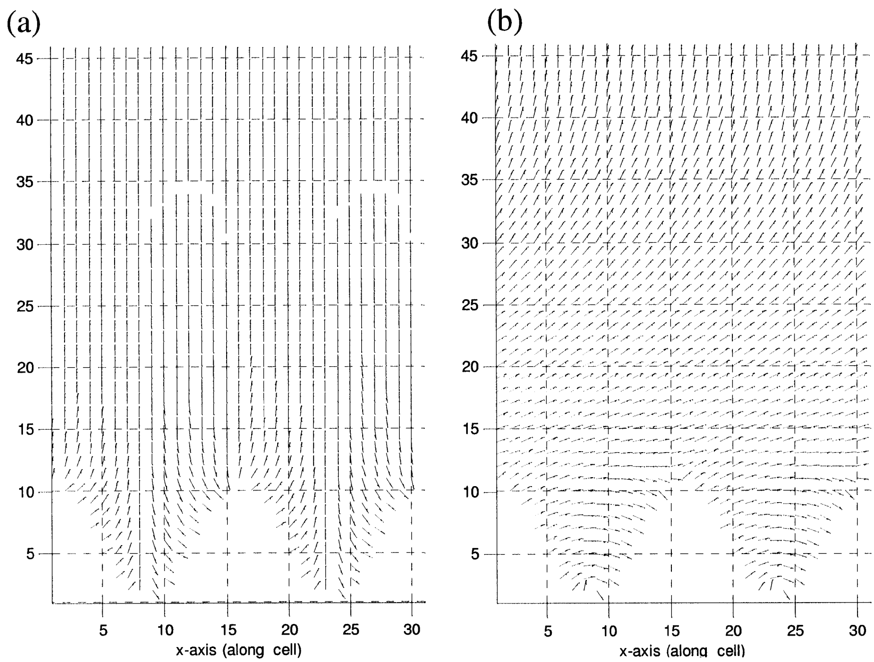

FIGURE 1 Stable director configurations on a sinusoidal grating (a) the defect-free state (b) the defect-containing state.

DIRECTOR PROFILE MODELLING

To model both stable states in these devices, it is necessary for the simulation to allow for the presence of defects. This is achieved by including the +/− n symmetry of the nematic. A convenient way of doing this is to use $\boldsymbol{Q}$, the tensor order parameter (see refs.[8,9]), in the formulation of the free energy expression. In this notation the elastic free energy equation for the one elastic constant approximation is rendered:

$$\boldsymbol{f}_s = \frac{\mathbf{1}}{\mathbf{9}}\boldsymbol{K}\frac{\boldsymbol{G}_1^{(2)}}{\boldsymbol{S}^2}$$

where $\boldsymbol{K}$ is the elastic constant, $\boldsymbol{S}$ is the scalar order parameter and

$$\boldsymbol{G}_1^{(2)} = \boldsymbol{Q}_{jk,l}\boldsymbol{Q}_{jk,l}$$

with

$$\boldsymbol{Q}_{jk} = \frac{\boldsymbol{S}}{\mathbf{2}}(\mathbf{3}\boldsymbol{n}_j\boldsymbol{n}_k - \boldsymbol{\delta}_{jk})$$
$$\boldsymbol{Q}_{jk,l} = \frac{\boldsymbol{\partial Q}_{jk}}{\boldsymbol{\partial l}}, \ldots \quad \boldsymbol{j},\boldsymbol{k},\boldsymbol{l} \in \{\boldsymbol{x},\boldsymbol{y},\boldsymbol{z}\}$$

$\boldsymbol{\delta}_{jk}$ is Kronecker's delta, $\boldsymbol{\delta_{jk}} = 1$ when $j = k$; otherwise $\boldsymbol{\delta_{jk}} = 0$ and $\boldsymbol{n}_i$ are the components of the director $\boldsymbol{n}$ (a unit vector).

The minimum energy state is calculated by solving the Euler-Lagrange equations for each director component subject to the constraint $|\boldsymbol{n}| = 1$.

The director configuration is found using a relaxation scheme:

$$\gamma_1 \frac{\boldsymbol{\partial}}{\boldsymbol{\partial t}}\boldsymbol{n}_i = -[\boldsymbol{f}_s]_{n_i} + \boldsymbol{\lambda n}_i$$

where γ_1 is the rotational viscosity.

$[\boldsymbol{f}_s]_{n_i}$ is the Euler-Lagrange Equation for the director component $\boldsymbol{n}_i$:

$$[\boldsymbol{f}_s]_{n_i} = \frac{\boldsymbol{\partial f}_s}{\boldsymbol{\partial n}_i} - \frac{\boldsymbol{d}}{\boldsymbol{dx}}\left(\frac{\boldsymbol{\partial f}_s}{\boldsymbol{\partial n}_{i,x}}\right) - \frac{\boldsymbol{d}}{\boldsymbol{dy}}\left(\frac{\boldsymbol{\partial f}_s}{\boldsymbol{\partial n}_{i,y}}\right) - \frac{\boldsymbol{d}}{\boldsymbol{dz}}\left(\frac{\boldsymbol{\partial f}_s}{\boldsymbol{\partial n}_{i,z}}\right)$$

$[\boldsymbol{f}_s]_{n_i}$ can be expressed in terms of $[\boldsymbol{f}_s]_{Q_{jk}}$ using the chain rule:

$$[\boldsymbol{f}_s]_{n_i} = [\boldsymbol{f}_s]_{Q_{jk}}\frac{\boldsymbol{\partial Q}_{jk}}{\boldsymbol{\partial n}_i} = [\boldsymbol{f}_s]_{Q_{jk}}\frac{\mathbf{3}\boldsymbol{S}}{\mathbf{2}}(\boldsymbol{n}_j\boldsymbol{\delta}_{ki} + \boldsymbol{n}_k\boldsymbol{\delta}_{ji})$$

Discretizing the relaxation scheme gives,

$$\gamma_1 \frac{\boldsymbol{\Delta n}_i}{\boldsymbol{\Delta t}} = -[\boldsymbol{f}_s]_{n_i} + \boldsymbol{\lambda n}_i$$
$$\boldsymbol{\Delta n}_i = -\frac{\Delta t}{\gamma_1}\left([\boldsymbol{f}_s]_{n_i} - \boldsymbol{\lambda n}_i\right)$$

The Lagrange multiplier can be neglected by renormalizing $\boldsymbol{n}$ at each time step. This results in a scheme where the director $\boldsymbol{n}^{\tau+1}$ at time $\tau + 1$ is calculated in a two-step process:

$$\tilde{\boldsymbol{n}}_i^{\tau+1} = \boldsymbol{n}_i^{\tau} - \frac{\Delta \boldsymbol{t}}{\gamma_1}[\boldsymbol{f}_s]_{n_i}^{\tau}$$

$$\boldsymbol{n}_i^{\tau+1} = \frac{\tilde{\boldsymbol{n}}_i^{\tau+1}}{|\tilde{\boldsymbol{n}}^{\tau+1}|}$$

Examples of the director profiles achieved using this approach are shown in Figure 1. To model the director profile for the cell used in the experiments, the grating profile was input into the director modelling code using a digitised Scanning Electron Microscope image of the grating. The diffraction from the profiles was then modelled using the FDTD method [7].

OPTICAL PROPERTIES OF GRATING CONTAINING CELLS

A cell containing a surface relief grating was fabricated at HP labs. The grating was written in a photoresist using photolithography. The internal surfaces of the cell were treated with a chromium complex to give homeotropic alignment. Using the experimental arrangement shown in Figure 2 we measured the strength of the +/− 1st diffracted orders and the 0th order.

The first polariser gave linearly polarised light of arbitrary polarisation. Passing this through a quarter-wave plate gave circularly polarised light. The second polariser then gave the required incident polarisation with each selected polarisation having the same intensity. The cell was mounted on a rotation stage thus allowing the incident angle to be varied. The photodetector was movable in order to record the strength of each of the diffraction spots in turn. The strength of diffraction was quantified using a diffraction efficiency 1st order/0th order, expressed as a percentage.

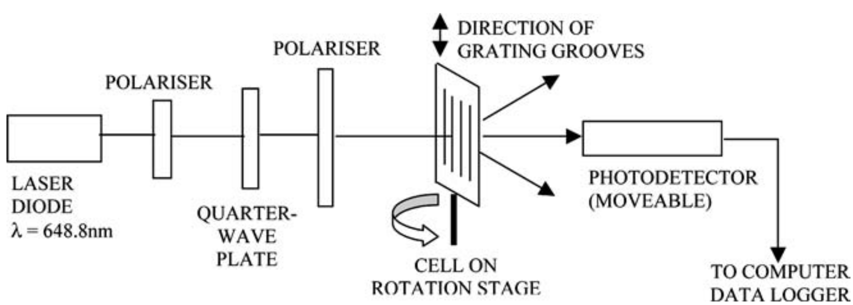

FIGURE 2 Experimental arrangement for measuring the diffraction from the cells.

Diffraction as a function of incident angle

The experimental results for diffraction efficiency as a function of incident angle are shown in Figures 3–6. Polarisations parallel to the grating grooves and normal to the grating grooves are used with both of the stable states.

It can be seen that the graphs for the two states with incident polarisation parallel to the grating grooves (Figs. 3 & 4) are practically identical. This is to be expected since for this polarisation the light will interact with n_o in both states. For the polarisation normal to the grating grooves, it can be seen that the defect-containing state has very low diffraction efficiency for the whole range of incident angles (Fig. 5). This is due to the effective refractive index of the liquid crystal being very similar to that of the grating. The liquid crystal material used was ZLI-2293 which has $n_o = 1.449$ and $n_e = 1.631$, while for the grating $n \approx 1.68$. In the defect

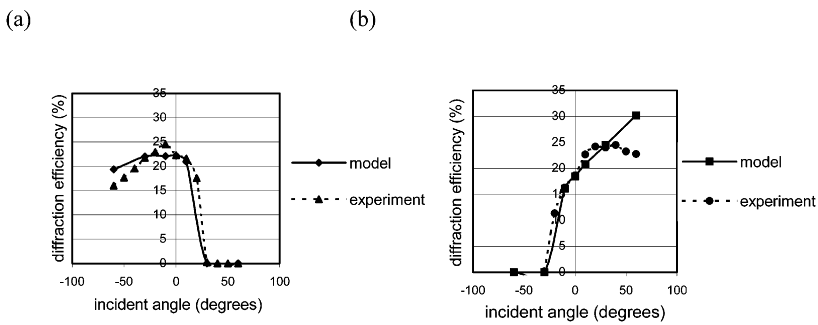

FIGURE 3 Variation in diffraction efficiency with incident angle for polarisation parallel to the grating grooves – the defect containing state (a) –1st order (b) 1st order.

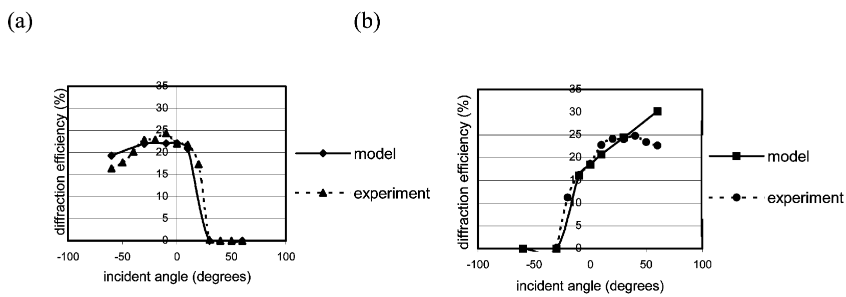

FIGURE 4 Variation in diffraction efficiency with incident angle for polarisation parallel to the grating grooves – the defect free state (a) –1st order (b) 1st order.

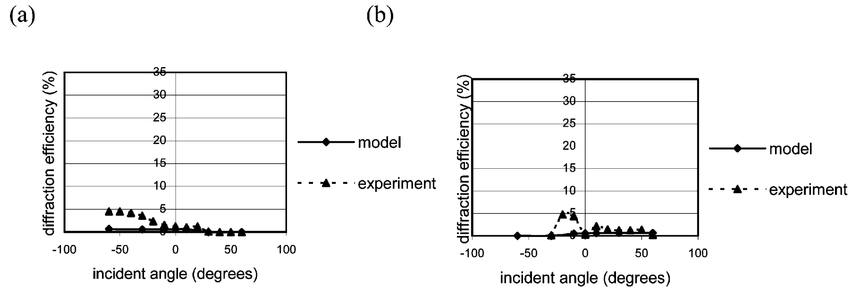

FIGURE 5 Variation in diffraction efficiency with incident angle for polarisation normal to the grating grooves – the defect-containing state (a) –1st order (b) 1st order.

state, the liquid crystal refractive index presented to the incident light in this polarisation is dominated by n_e and therefore the mismatch to the grating is small.

The modelled results are also shown in Figures 3–6. It can be seen that there is reasonable agreement between the experiment and the model, particularly when comparing the trends in behaviour with different polarisations.

The results for varying incident polarisation are shown in Figures 7 & 8. It can be seen that the diffraction efficiency varies smoothly as a function of incident polarisation. This is in agreement with the modelled results also shown in Figures 7 & 8. As incident polarisation is varied, the effective refractive index presented to the light is altered. This in turn changes the effective refractive index mismatch to the grating and hence we see a change in diffraction efficiency. The change in diffraction efficiency for the defect-free state is smaller than that for the defect-containing state.

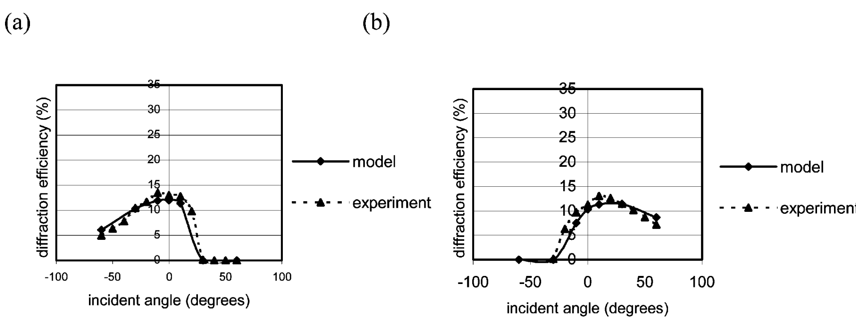

FIGURE 6 Variation in diffraction efficiency with incident angle for polarisation normal to the grating grooves – the defect-free state (a) –1st order (b) 1st order.

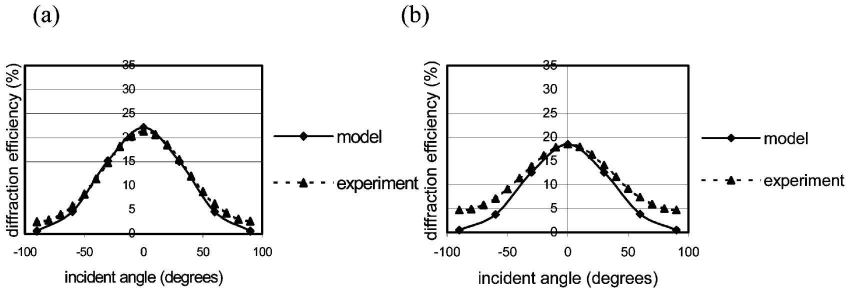

FIGURE 7 Variation in diffraction efficiency with incident polarisation – the defect containing state (a) –1st order (b) 1st order.

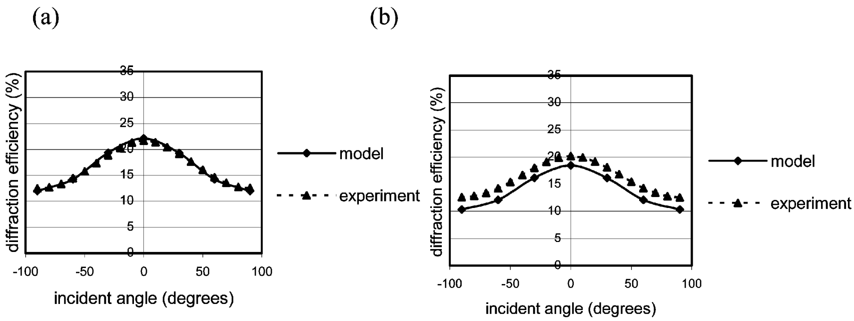

FIGURE 8 Variation in diffraction efficiency with incident polarisation – the defect free state (a) –1st order (b) 1st order

This is because in the defect-free state the director is nearly parallel to the direction of propagation of the light. Thus all polarisations interact with a refractive index that is largely composed of n_o and has only a small, approximately constant contribution from n_e.

The disparity between the experimental and modelled results may be due to the digitisation of the grating shape. There is also some uncertainty in the refractive index of the photoresist since this is likely to change from the manufacturer's quoted value during the processing used to ruggedise the grating. Here we have used an estimate for the refractive index based on the diffraction strength of a typical grating measured in air.

CONCLUSIONS

We have demonstrated that the diffraction from zenithal bistable nematic cells is sensitive to incident polarisation. We have also shown that diffraction strength varies with incident angle. Our simulations have shown we can model this optical behaviour. We postulate that the overall optical characteristics of these devices may be influenced by the polarisation and incident angle of the illumination, an important consideration when constructing an operational device. It may also be possible to gain more detailed information on the director structure using techniques similar to those used here and this point will be further investigated in the future.

REFERENCES

[1] Bryan-Brown, G. P., Brown, C. V., Jones, J. C., Wood, E. L., Sage, I. C., & Brett, P. (1997). *SID Digest*, *XXVIII*, 37.

[2] Bryan-Brown, G. P., Wood, E. L., Brown, C. V., Jones, J. C., Sage, I. C., & Brett, P. (1997). *SID proc. 4th Int. Display Workshop*, 261.

[3] Newton, C. J. P. & Spiller, T. P. (2001). *Mol. Cryst. and Liq. Cryst.*, *372*, 167.

[4] Bryan-Brown, G. P., Wood, E. L., & Jones, J. C. (1998). *Proceedings of Asia Display (SID)*, 1051.

[5] Jones, J. C., Graham, A., Bryan-Brown, G., Wood, E., & Brett, P. (2000). *Proceedings of ASET International Forum on Low Power Displays*, 19.

[6] Edwards, E. G., Brown, C. V., Kriezis, E. E., & Elston, S. J. (2001). *Proceedings of the 2nd Anglo-Japanese Seminar on Liquid Crystals 2001 (Mol. Cryst. and Liq. Cryst) – to be published.*

[7] Kriezis, E. E., Flippov, S. K., & Elston, S. J. (2000). *J. Opt. A: Appl. Opt.*, *2*, 27.

[8] Mori, H., Gartland Jr., E. C., Kelly, J. R., & Bos, P. J. (1999). *Jpn. J. Appl. Phys.*, *38*, 135.

[9] Denniston, C. & Yeomans, J. M. (2001). *Phys. Rev. Lett.*, *87*(27).